doi:10.1006/jmbi.2001.5330 available online at http://www.idealibrary.com on IDEAL® J. Mol. Biol. (2002) 316, 201–211

JMB

A Structural Model for the Catalytic Cycle of Ca^{2+}-ATPase

Chen Xu†, William J. Rice†, Wanzhong He and David L. Stokes*

Skirball Institute for Biomolecular Medicine Department of Cell Biology New York University School of Medicine, 540 First Ave, New York, NY 10016, USA

Ca^{2+}-ATPase is responsible for active transport of calcium ions across the sarcoplasmic reticulum membrane. This coupling involves an ordered sequence of reversible reactions occurring alternately at the ATP site within the cytoplasmic domains, or at the calcium transport sites within the transmembrane domain. These two sites are separated by a large distance and conformational changes have long been postulated to play an important role in their coordination. To characterize the nature of these conformational changes, we have built atomic models for two reaction intermediates and postulated the mechanisms governing the large structural changes. One model is based on fitting the X-ray crystallographic structure of Ca^{2+}-ATPase in the E1 state to a new 6 Å structure by cryoelectron microscopy in the E2 state. This fit indicates that calcium binding induces enormous movements of all three cytoplasmic domains as well as significant changes in several transmembrane helices. We found that fluorescein isothiocyanate displaced a decavanadate molecule normally located at the intersection of the three cytoplasmic domains, but did not affect their juxtaposition; this result indicates that our model likely reflects a native E2 conformation and not an artifact of decavanadate binding. To explain the dramatic structural effect of calcium binding, we propose that M4 and M5 transmembrane helices are responsive to calcium binding and directly induce rotation of the phosphorylation domain. Furthermore, we hypothesize that both the nucleotide-binding and β-sheet domains are highly mobile and driven by Brownian motion to elicit phosphoenzyme formation and calcium transport, respectively. If so, the reaction cycle of Ca^{2+}-ATPase would have elements of a Brownian ratchet, where the chemical reactions of ATP hydrolysis are used to direct the random thermal oscillations of an innately flexible molecule.

Keywords: Ca^{2+}-ATPase; ion transport; electron microscopy; atomic modelling; energy coupling

*Corresponding author

Introduction

P-type ion pumps are responsible for active transport of cations across a wide variety of cellular membranes.[1] The functional core of these pumps appears to be a single polypeptide that couples ion binding and release in the transmembrane domain with ATP hydrolysis in a cytoplasmic domain.[2] The catalytic cycle involves a number of distinct conformations that serve to couple events in the transmembrane domain with those in the cytoplasmic domains.[3] Ca^{2+}-ATPase is a well-studied archetype for this family; its catalytic cycle starts with the binding of cytoplasmic calcium ions along the transmembrane helices, which elicits phosphorylation of an aspartate residue in a highly conserved region of a cytoplasmic domain. Calcium-binding and phosphorylation sites are separated by ~40 Å, according to the recently reported X-ray crystal structure of Ca^{2+}-ATPase,[4] and a variety of spectroscopic and biochemical experiments suggest that a global conformational change is used for coupling.[5] In the next step, the chemical energy of the aspartyl phosphate group induces a further conformational change, which lowers ion affinity drastically and switches ion

†These authors contributed equally to this work.

Present address: C. Xu, Rosenstiel Center, Brandeis University, Waltham, MA 02454, USA.

Abbreviations used: cryoEM, cryoelectron microscopy; FITC, fluorescein isothiocyanate.

E-mail address of the corresponding author: stokes@saturn.med.nyu.edu

0022-2836/02/010201–11 $35.00/0

accessibility from cytoplasmic to lumenal (extracellular) sides of the membrane. Finally, the release of Ca^{2+} from their transmembrane binding sites signals the hydrolysis of the aspartyl phosphate group, thus returning the pump to the beginning of the cycle.

Structural studies have so far defined the structure of two intermediates in this reaction cycle. Electron microscopy has been used to determine a structure at 8 Å resolution of Ca^{2+}-ATPase inhibited with decavanadate and thapsigargin in the Ca^{2+}-free (E2) state.[6–8] X-ray crystallography has produced an atomic structure of Ca^{2+}-ATPase in the presence of saturating concentrations of Ca^{2+} (E1 state).[4] Consistent with spectroscopic studies on the effect of Ca^{2+},[9] comparison of these structures reveals dramatic differences in the arrangement of the three cytoplasmic domains. It is likely that these differences reflect the structural mechanism by which the aspartate residue is activated for phosphate transfer.

Here, we present two new structures of the E2 form of Ca^{2+}-ATPase determined by cryoelectron microscopy (cryoEM). One of these structures improves the resolution to 6 Å and is used for building an atomic model for the E2 state by fitting atomic coordinates of individual domains from the E1 state. The other structure was determined after labelling Ca^{2+}-ATPase with fluorescein isothiocyanate (FITC) and shows that such labelling excludes decavanadate from its intramolecular binding site at the intersection of the three cytoplasmic domains. The latter structure indicates that decavanadate does not have a significant effect on the juxtaposition of cytoplasmic domains and therefore that the enormous movements suggested by our model are an innate property of Ca^{2+}-ATPase, not an artifact of the decavanadate used for crystallization.

Results

The 6 Å structure of native Ca^{2+}-ATPase by cryoelectron microscopy

Our primary goal was to fit the atomic coordinates for Ca^{2+}-ATPase in the Ca^{2+}-bound, E1 state to the cryoEM structure for the Ca^{2+}-free, E2 state. To maximize our confidence in this fit, we have improved the resolution of our structure to 6 Å, primarily by increasing the number of tubular crystals included in the final data set (Table 1). These crystals fell into five different symmetry groups with 7-21 tubes in each group. Data within each group were averaged in Fourier space and were used to calculate 3D maps. Individual molecules were masked from these maps, aligned and then averaged in real space. We used three different measures of resolution: 2-fold phase residual, Fourier shell correlation and phase comparison between half data sets (Figure 1). At 6 Å resolution, our correlation coefficient and phase residual are similar to criteria reported for the 4.6 Å structure of nicotinic acetylcholine receptor (0.3 and 60°, respectively).[10] After averaging, maps were back-transformed and Fourier data along the layer-lines were filtered based on local 2-fold phase residual; data with errors >65° were removed, which comprised 25% of data in the highest-resolution bin. This filtering improved 2-fold phase residual perceptibly (compare Table 1 with Figure 1), but had no effect on the more objective comparisons between the half data sets (Figure 1), which are most likely dominated by the remaining, higher-amplitude data. Nevertheless, we believe that this filter suppressed noise in the map, which was helpful when applying a moderate inverse temperature factor (50-100 Å^2) to accentuate higher-resolution features corresponding to elements of secondary structure.

Table 1. Statistics of data merging

	Native tubes						FITC-labelled tubes		
	(−23,6)[a]	(−22,6)	(−21,6)	(−20,6)	(−19,6)	Avg	(−21,6)	(−22,6)	Avg
No. tubes[b]	7/6	21/19	13/9	15/14	14/10	70/58	7/7	5/5	12/12
No. repeats[b]	9/8	41/38	22/17	20/19	17/13	109/95	15/15	7/7	22/22
a/*b* (Å)	57.9/115.9	56.9/117.1	57.0/116.7	56.3/118.0	56.6/117.6		57.4/121.6	57.3/120.4	
γ (deg.)	65.2	64.2	63.95	63.0	63.0		62.9	63.6	
Resoln (Å)	2-Fold residual[c] (°)								
40	4.22	1.31	1.75	5.83	5.40	1.08	3.25	5.96	1.51
30	5.97	2.50	2.97	7.64	5.54	1.70	4.30	8.73	2.53
20	14.65	6.56	8.58	13.33	15.73	4.00	19.69	20.87	10.25
14	33.65	24.36	32.27	30.37	30.40	15.25	32.54	38.43	24.63
10	41.81	34.74	38.63	41.54	40.38	27.51	40.98	42.10	35.73
8	43.93	44.31	45.70	44.20	43.95	37.24	44.16	44.89	43.54
6	44.59	45.01	45.78	44.79	45.24	44.64	-	-	-

[a] Symmetry of each family characterized by the Bessel order (*n*) of the (1,0) and (0,1) layer-lines.
[b] Numbers correspond to those processed and those used after considering unit cell parameters of individual tubes (see Materials and Methods).
[c] The 2-fold phase statistics were calculated prior to filtering and include all layer-line data. Compare with 2-fold statistics in Figure 1 for effect of filtering.

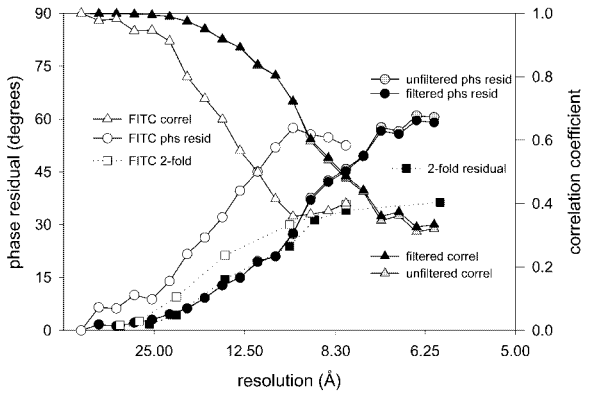

Figure 1. Statistics of data averaging for tubular crystals of native Ca^{2+}-ATPase (grey and black symbols) and FITC-labelled Ca^{2+}-ATPase (white symbols). Three different parameters were used to assess resolution. Independent, half data sets were compared to determine correlation coefficients (triangles) and phase residuals (circles) both before (grey) and after (black) applying a filter to remove layer-line data with a local phase error >65°. In addition, 2-fold phase residuals (squares) were determined directly from layer-line data; 2-fold residuals plotted here were calculated after the filter, whereas those in Table 1 were calculated before the filter. Although this filter improved 2-fold statistics at high resolution, it didn't have much effect on phase residual or correlation coefficients from the half data sets.

Structure of FITC-labelled Ca^{2+}-ATPase

In addition to this 6 Å structure of native Ca^{2+}-ATPase, we have determined a new structure of FITC-labelled Ca^{2+}-ATPase. This covalent inhibitor specifically labels Lys515 within the ATP-binding pocket and prevents ATP binding;[11] its fluorescent signal has been used extensively to monitor conformational changes.[9] FITC was reported to reduce the stoichiometry of decavanadate binding to Ca^{2+}-ATPase;[12] however, despite the requirement of decavanadate for formation of tubular crystals,[13] FITC does not prevent crystallization.[14] We have therefore determined the structure of FITC-labelled Ca^{2+}-ATPase to distinguish the relative contributions of decavanadate to crystallization and to Ca^{2+}-ATPase conformation.

For our structure of FITC-labelled Ca^{2+}-ATPase, we averaged 12 tubes from two different symmetry groups. The phase statistics and Fourier shell correlation suggest a resolution of 8-10 Å (Table 1, Figure 1). The structure itself is largely similar to native Ca^{2+}-ATPase, except for the striking absence of a strong density peak at the intersection of the three cytoplasmic domains (Figure 2). This absence is consistent with our previous assignment of this peak to decavanadate.[15] A second, spherical density remains on the 2-fold axis of these 2D crystals and is consistent with the presence of a second decavanadate molecule mediating the intermolecular contacts. This result explains how FITC labelling reduces decavanadate stoichiometry from 1.5 to 0.5 without preventing crystal formation.[12]

Fitting of atomic coordinates to density maps

Even a casual comparison of cryoEM maps to the atomic coordinates for Ca^{2+}-ATPase indicates that the cytoplasmic domains undergo a radical rearrangement during the transition from the E_2 to the E_1 conformation. Thus, rigid-body docking of the entire Ca^{2+}-ATPase molecule produces a very poor fit. We therefore divided the molecule into four different domains based on three likely hinges (see Materials and Methods). The three cytoplasmic domains, designated N for nucleotide binding, P for phosphorylation and β for β-barrel, were then

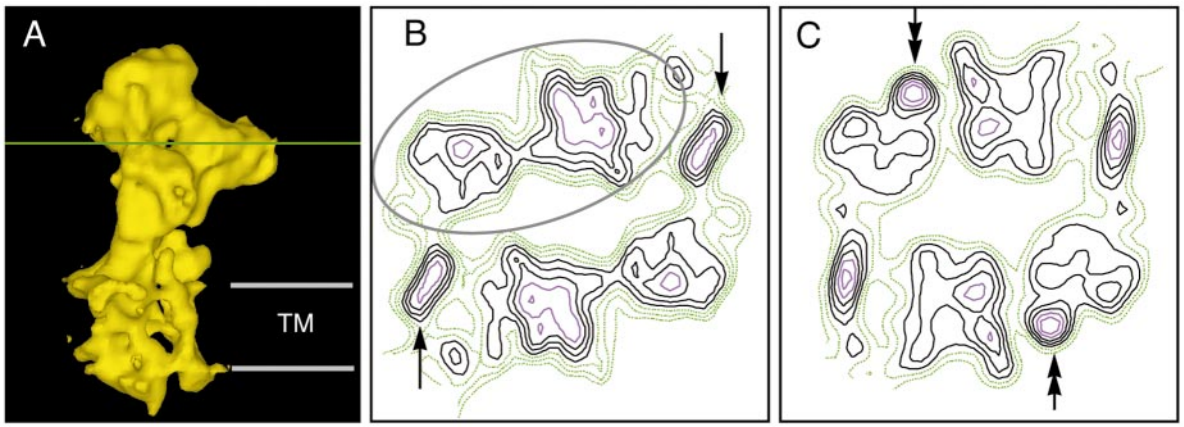

Figure 2. FITC labelling displaces decavanadate from intramolecular, but not intermolecular binding sites. (a) Surface rendering of our 3D reconstruction of FITC-labelled Ca^{2+}-ATPase with a distinct hole in the middle of the cytoplasmic head, which is intersected by the horizontal, green line. Grey horizontal lines indicate the borders of the membrane. (b) and (c) Sections through the maps of FITC-labelled and native Ca^{2+}-ATPase, respectively, at the level indicated by the green line in (a). A single Ca^{2+}-ATPase from the *p*2 lattice is circled in grey and density peaks from intermolecular decavanadate molecules are indicated by arrows in (b). Density peaks from the intramolecular decavanadate molecule is indicated by the double arrowhead in (c).

docked as independent rigid bodies to the cryoEM density map of native Ca^{2+}-ATPase using both manual manipulation (O[16]) and automated fitting (SITUS[17]). Although similar results could be obtained, the manual methods were more satisfactory in matching secondary structure to particular densities in the map and in obtaining the highest correlation coefficient. This is likely due to the strategy for automated fitting, which represents both the map and the coordinates as a small number of codebook vectors. This strategy matches the density outline relatively well, but does not consider local densities that correspond to elements of secondary structure. After our manual fitting, our cryoEM density map is well fit in terms of both core secondary structure and loops at the periphery of the domains (Figure 3). Only the extremely flexible loops connecting the β-domain with the

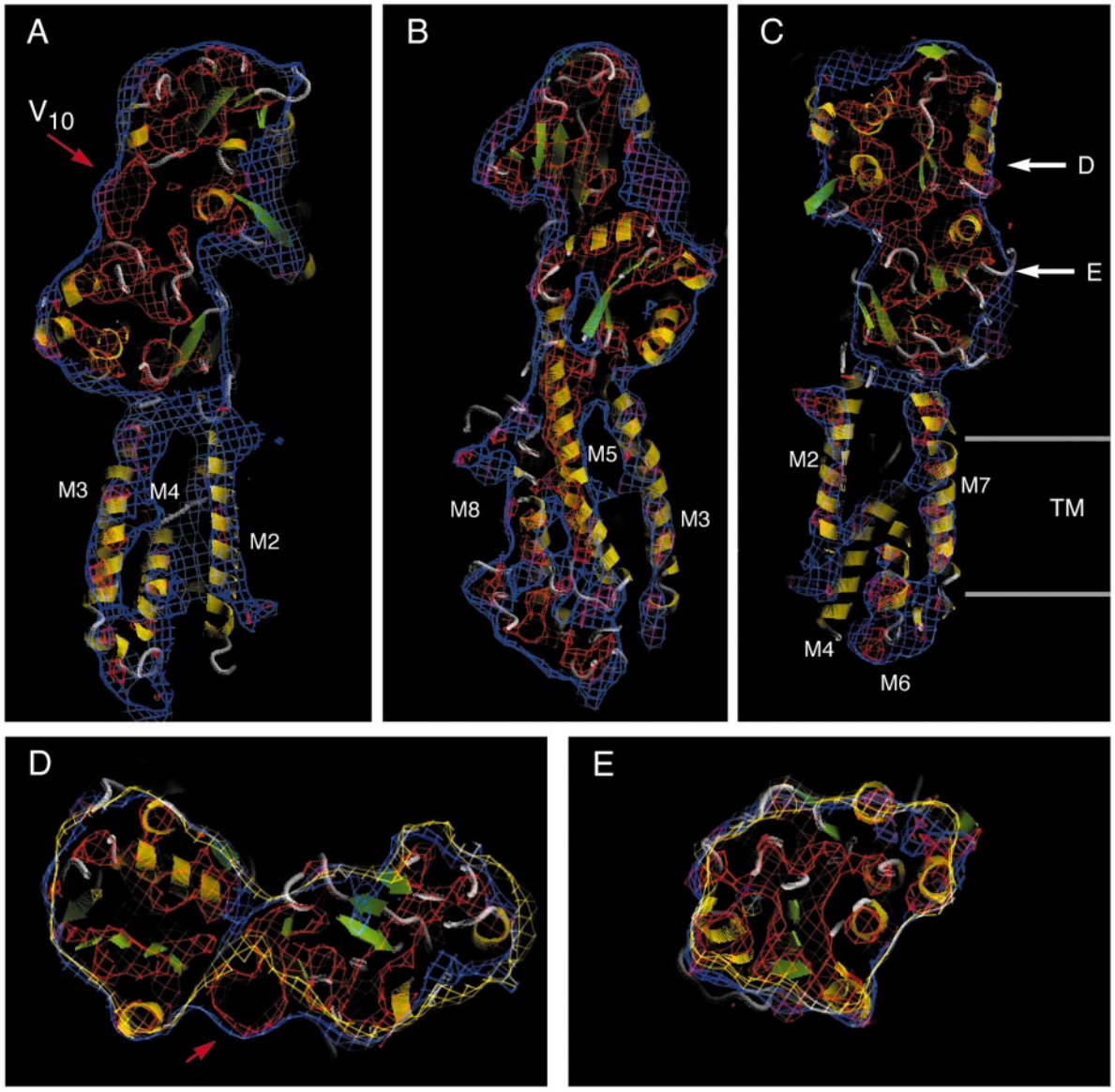

Figure 3. Fitting of the density map of native Ca^{2+}-ATPase with atomic coordinates. (a)-(c) Sections perpendicular to the membrane showing transmembrane helices, P and N-domains. Although the detailed fitting of secondary structure to cytoplasmic domains is difficult to appreciate from these static views, the overall fit of the envelope is clear. (d) Cross-section through the N-domain (left) and β-domain (right) at the level of intramolecular decavanadate, which is indicated by the red arrow in (a) and (d). (e) Cross-section through the P-domain just below D351. The blue and red density envelopes correspond to native Ca^{2+}-ATPase at two different density cutoffs (red has an inverse temperature factor of 50 $Å^2$), whereas the yellow envelope in (d) and (e) corresponds to FITC-labelled Ca^{2+}-ATPase. Thus, FITC does not affect domain orientation appreciably, despite its complete displacement of the intramolecular decavandate. Labelled arrows in (c) indicate the level of the sections in (d) and (e), and TM indicates the transmembrane region.

transmembrane helices M1 and M3 fall outside visible density, though the connection with M2 represents a new feature that is resolved in this 6 Å map. The resulting structural changes involve a 53° rotation of the P-domain about an oblique axis and a 90° rotation of the β-domain about an axis perpendicular to the membrane; the N-domain rotates with the P-domain and is therefore displaced by up to 50 Å at the top of the molecule.

Unlike the rigid-body docking of cytoplasmic domains, individual helices in the transmembrane and stalk domains were displaced or bent to follow the corresponding densities in the map. Given the well-defined helical densities in this part of the map (Figure 3(a)-(c)), these adjustments were generally unambiguous and done by manual manipulations of the coordinates. Currently, automated fitting programs are not designed to make such modifications to elements of secondary structure. As a result of our fitting, M2, M4 and M5 were modified significantly, whereas M1 and M6 required more minor changes. In particular, the entire length of M2 was inclined by ~14°, resulting in a 9 Å displacement of Trp107 at the cytoplasmic membrane surface and a 13.5 Å displacement of Ala118 near the bottom of the β-domain. The upper part of M4, above Pro312, was displaced laterally by 4-5 Å and the lower third of M5 was bent below Asn768 by ~20°, resulting in a 6.5 Å displacement of Ala 780. M1 was bent at the cytoplasmic membrane surface to fill a strong map density there and the upper part of M6 was bent at Gly801. In addition, M8 was inclined slightly and M10 was displaced somewhat, but map densities for these latter two helices were not as well defined.

After fitting the four principal domains, the hinges were rebuilt in order to restore the connections. Except for the connection between M4/M5 and the P-domain, these hinges consist of flexible, unstructured loops in the X-ray structure, so this rebuilding simply involved bending the loops to reconnect the loose ends. Despite the dramatic rearrangements of the cytoplasmic domains, the lengths of these loops were just sufficient for such reconnection. In reconnecting M4 and M5 to the P-domain, the latter was bent above Ala752 to fit within well-defined density and otherwise required only minor modification to Phe740 to complete the connection. In the case of M4, the topmost residues, Lys328 and Lys329, were unwound from their α-helix, which had been moved down by 4.5 Å; without these changes, M4 would protrude significantly from the cryoEM density map.

A very strong, spherical density at the intersection of the three cytoplasmic domains is not accounted for by the remodelled atomic coordinates. This density was previously assigned to decavanadate and this assignment is now supported strongly by the map of FITC-labelled Ca^{2+}-ATPase, from which this density peak is completely absent. Despite its absence, the disposition of cytoplasmic domains in this latter structure is virtually identical with that from unlabelled Ca^{2+}-ATPase (Figure 3(d)-(e)), illustrating that decavanadate is not influencing the disposition of these cytoplasmic domains overtly. Overall, the fit can be characterized by the cross-correlation coefficient between the experimental map and the corresponding map generated from the atomic model, which was calculated by SITUS to be 0.68; considering that the decavanadate density was not accounted for by our model, this value compares favorably with the that of 0.76 for fitting of EF-G.[18]

Discussion

E_1 and E_2 conformations

Comparison of the published atomic coordinates for Ca^{2+}-ATPase in the E1 state with our modelled coordinates in the E2 state illustrates the global change in molecular structure that characterizes the E2 to E1 conformational change. This conformational change has been studied extensively by biochemical and spectroscopic methods, which have documented alterations in proteolytic patterns, in fluorescent efficiencies of various probes and in chemical reactivities.[5,9] The physiological substrate is, of course, ATP, and change in its reactivity represents one of the keys to energy coupling. In particular, even though the E2 conformation binds ATP readily, phosphate transfer to D351 occurs only after the binding of cytoplasmic Ca^{2+} elicits the transition to the E1 conformation. The chemical energy of this aspartyl phosphate group is used in a subsequent step to reorient the Ca^{2+} sites towards the lumen and to reduce their affinity substantially, thus achieving Ca^{2+} transport against a concentration gradient.[19]

Our assignment of the E1 and E2 conformation to these two atomic models relies on the conditions required to grow the respective crystals.[14] The 3D crystals used for X-ray crystallography were grown in the presence of saturating concentrations of Ca^{2+}, consistent with stabilization of E1. In contrast, our 2D tubular crystals were grown in the presence of EGTA and are disrupted by micromolar concentrations of Ca^{2+}, suggesting that they require the E2 conformation. This interpretation is complicated by the use of vanadate to induce crystallization; although decavanadate appears to be the effective species,[13] orthovanadate is present in these solutions and could potentially act as an analogue for orthophosphate to stabilize a transition state in the hydrolysis of E2-P. A recent proteolysis study reported that ligands stabilizing E2-P (MgF, VO_4, PO_4) reduced the rate of proteolysis and, furthermore, that decavanadate/EGTA produces proteolytic rates resembling E2-P.[20] Curiously, thapsigargin was reported to have little effect on these rates, despite its well-documented capacity to stabilize E2.[21] One explanation for these observations is that thapsigargin affects mainly the transmembrane domain, where Ca^{2+} binds, whereas cytoplasmic domains are dynamic in the

absence of relevant ligands and therefore more susceptible to proteolysis. However, it should be noted that the proteolytic susceptibility of E2 is still very low compared to E1, suggesting that E2 and E2-P may be relatively similar.[22] Indeed, scallop Ca^{2+}-ATPase readily forms identical tubular crystals in EGTA alone (E2),[23] whereas conditions that generate E2-P have been shown to generate a different crystal form.[24]

Domain movements

The three cytoplasmic domains have dramatically different arrangements in the two structures. The P-domain has rotated about both vertical and out-of-plane axes in the view in Figure 4, significantly reorienting the catalytic site, which lies on a plane along the top of this Rossmann fold. In addition to this reorientation, there are probably local changes at the catalytic site that make D351 reactive towards either ATP or a variety of other high-energy phosphate-containing molecules, such as acetylphosphate and *p*-nitrophenolphosphate.[25] Although the N-domain undergoes a substantial displacement (~50 Å for the uppermost residues), this movement is almost entirely due to movement of the P-domain. Thus, the physical relationship between N and P-domains are not much different in the two structures. The β-domain rotates ~90° about a vertical axis, thus engaging the conserved TGES sequence with the catalytic site in the E2 conformation (see Figure 6). In E1, the whole β-domain has little contact with the rest of the molecule and the tryptic cleavage site at R198 (T2) is freely accessible, as expected from its increased susceptibility.[5] Within the transmembrane domain, movements are much less dramatic, the largest displacement being ~10 Å for M2 and M10. Other significant displacements occur along the upper parts of M1 and M4 and either end of M5 as detailed in Results. Overall, our model appears to be similar to that presented by Toyoshima *et al.*,[4] though careful examination of their model coordinates (1FQU) shows significant differences due to the magnification factor they applied prior to fitting and a slightly different orientation of the P-domain.

Structural effects of Ca^{2+} binding

From this comparison, it seems clear that M4 and M5 relay the effects of Ca^{2+} binding to the P-domain and elicit its rotation and consequent increase in reactivity. Indeed, our model for the E2 state reveals significant movements of the helical segments at the top of M4 and M5, which are well positioned to leverage the P-domain rotation (Figure 4(c)). Given that Ca^{2+} binding elicits the movement, the motor logically resides amongst the residues composing the Ca^{2+}-binding sites. In particular, the non-helical segment of M4 seems to be a likely candidate for structural changes, given its structural conservation across the family of P-type pumps and its direct connection to the putative

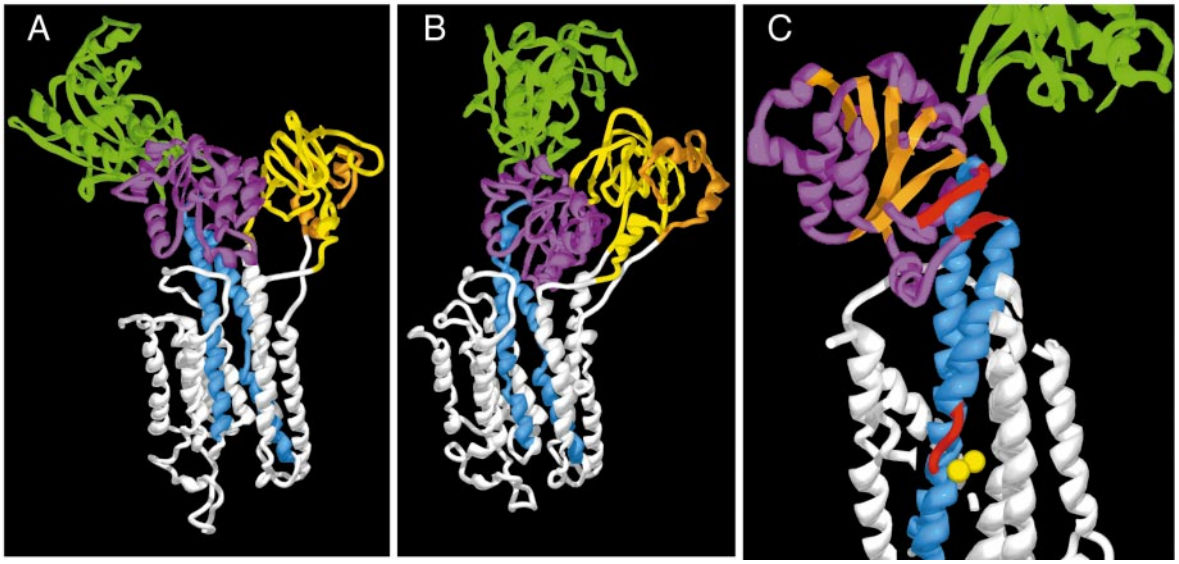

Figure 4. Atomic models for E1 and E2 states. (a) Coordinates from the X-ray structure 1EUL with N-domain colored green, P-domain magenta, transmembrane helices white, except for M4 and M5, which are blue, and β-domain yellow, except for the two N-terminal helices, which are orange. (b) Our model after fitting individual domains to the cryoEM density map in the E2 conformation. The P-domain has rotated by 53° about an oblique axis carrying the N-domain with it. The β-domain has rotated by 90° about a vertical axis. M2, M4, and M5 have undergone significant changes. (c) Closeup of the structural coupling between the calcium-binding sites along M4, M5 and the P-domain. The unwound region of M4 is colored red, as are the β-strands connected directly to the top of M4 and M5; these β-strands are part of the central β-sheet (orange) characterizing the Rossmann fold of the P-domain. The β-domain, M1, M2, and M3 have been removed by the clipping plane in (c).

lever arms. The X-ray structure of the E1 conformation shows that main-chain carbonyl groups in this unwound segment of M4 are ligands to the bound Ca^{2+}. Furthermore, the presence of two proline residues on either side of Glu309 destabilizes this ''transmembrane helix''. One possibility is that this region of M4 adopts a partially helical structure in the E2 state and that Ca^{2+} binding to the main-chain carbonyl groups instigates an unwinding or extension of this region, thus motivating the observed conformational change.

Phosphorylation by ATP

The ATP-binding site in the N-domain has been identified by a crystallographic difference map, by chemical labelling and by site-directed mutagenesis. However, this ATP site is >25 Å away from D351 in the X-ray structure in the E1 state, implying that a further conformational change is required for phosphate transfer. Rather than a deliberate conformational change, we propose that the N-domain is actually quite flexible and susceptible to Brownian motion. Thus, the X-ray crystal structure represents only one of many possible configurations of the N-domain in the E1 state, which happens to be stabilized by the intermolecular contacts stabilizing this particular crystal form. In support of this idea, the structure of H^+-ATPase shows the N-domain in a more vertical position,[26] as does a projection structure of Ca^{2+}-ATPase in related crystals with a different unit-cell geometry.[27] Given such flexibility, Brownian motion could periodically bring the N-domain in close proximity to the P-domain and, when encountering an activated D351, would allow rapid transfer of phosphate from ATP.

To investigate the plausibility of this hypothesis, we have modelled the Brownian motion of the N-domain by rotation about the two strands connecting the N and P-domains. In particular, the unstructured loops near TNQM and the highly conserved DPPR were used as a pivot point to swivel the N-domain down towards the P-domain. This rotation was unhindered by steric clashes and effectively brings the ATP molecule docked in the N-domain into close physical proximity of D351 (Figure 5). Furthermore, this rotation closes the distance between the side-chains of K492 and R678 from 20.6 Å to 4.1 Å, which accounts for their observed crosslinking by glutaraldehyde in the E1 conformation.[28] This swiveling of the N-domain is unhindered largely because of the detached position of the β-domain in the E1 conformation. On the other hand, in our E2 model, the N-domain appears to interact with the rotated β-domain and is therefore constrained from moving closer to the P-domain, consistent with the decreased mobility observed for the N-domain in the E2 conformation.[29]

β-Domain rotation: a Brownian ratchet

Our models indicate that the β-domain undergoes a 90° rotation during the E2 to E1 conformational change (Figure 6) and there is some evidence to suggest that it rotates back during the $E1 \sim P$ to E2-P transition. In particular, Fe-catalyzed cleavage of Na^+,K^+-ATPase occurs when Fe is substituted for Mg at the active site and has been used to identify peptides in close proximity to the catalytic aspartate residue at various steps in the reaction cycle.[30] These studies show that the conserved TGES sequence in the β-domain is cleaved in the E2 and E2-P conformations, but not in E1 and $E1 \sim P$. From a structural point of view, it is difficult to envision how β-domain rotation could be accomplished, given the flexible loops connecting it to the transmembrane domain and the minimal van der Waals contact with either N or P-domains. Instead, we propose that this domain is flexible and that Brownian motion provides the energy for this rotation. In the context of the reaction cycle, we propose that the presence of the aspartyl phosphate group at the catalytic site provides a latch that catches the β-domain when it reaches the appropriate configuration. This idea is similar to proposals for myosin movement along actin[31] and to the proposed rotation of the c subunit ring in the Fo portion of ATP synthase.[32] Once stabilized, the new orientation of the β-domain would then put strain on the loops connecting to M1, M2, and M3, two of which are displaced substantially in E2 relative to E1 (Figure 6). M1 contributes directly to the Ca^{2+} sites *via* Glu55, whereas M2 could exert indirect affects, thus eliciting Ca^{2+} release to the lumen.

The final step in the reaction cycle involves hydrolysis of the aspartyl phosphate group, which occurs after Ca^{2+} release. This coupling implies that Ca^{2+} release allows some kind of relaxation amongst the transmembrane helices, which could be relayed to the P-domain *via* the M4 and M5 levers discussed above. The absence of phosphate would release the latch for the β-domain, presumably leaving it free to move. However, Fe-catalyzed cleavage of the TGES sequence is still observed in this E2 state,[30] suggesting that domain interactions may hold the β-domain in place, albeit more weakly, until binding of cytoplasmic calcium induces the large rotation of the P-domain.

Conclusion

We have hypothesized a specific structural mechanism for each of the conformational changes E_2 to E_1, E_1 to $E_1 \sim P$, and $E_1 \sim P$ to E_2-P (Figure 7). The former employs rigid mechanical coupling along the M4 and M5 helices, which transduces local changes at the calcium-binding site to P-domain rotation; the latter two steps rely on Brownian motion, using alterations in chemical surfaces to trap particular conformational states. We eagerly await future crystal

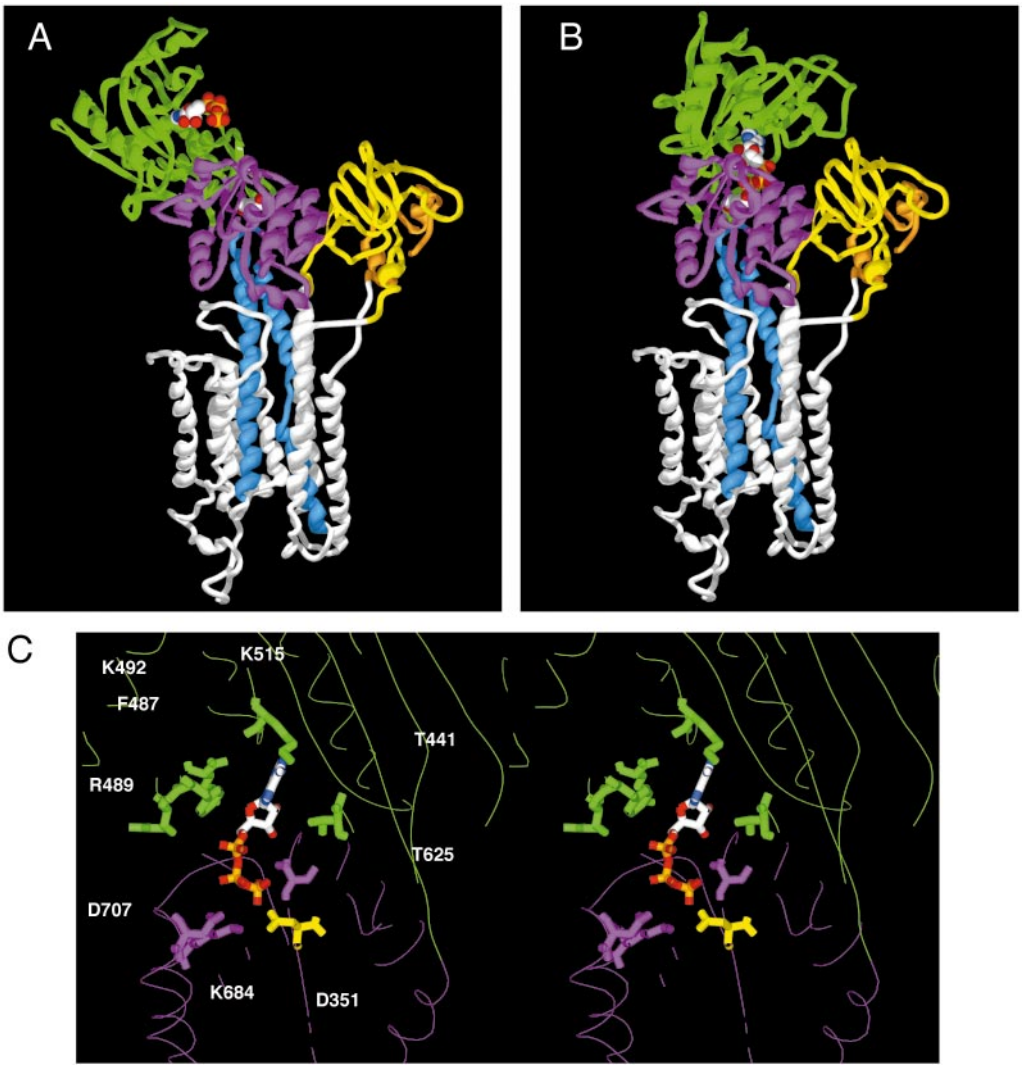

Figure 5. Hypothetical flexibility of the N-domain could allow for phosphoryl transfer to D351. (a) X-ray crystallographic structure 1EUL with ATP docked to the N-domain according to Figure 6 of Toyoshima *et al*.[4] Both ATP and the D351 side-chain are shown by CPK surfaces. (b) The same structure after rotating the N-domain about flexible hinges at N359 and R604. (c) Closeup stereo view of the ATP-binding pocket in (b), showing selected residues involved in ATP binding (green) and in phosphoryl transfer (magenta and yellow).

structures of the various reaction intermediates, which will specify the atomic interactions that stabilize domain interactions and hopefully support our hypotheses. In the meantime, our models may offer a template from which spectroscopic or mutagenesis experiments can start to address the dynamics that govern the reaction cycle of Ca^{2+}-ATPase and other P-type ion pumps.

Materials and Methods

Preparation and crystallization of Ca^{2+}-ATPase

Sarcoplasmic reticulum (SR) was prepared from the white muscle of rabbit hind legs by the method of Eletr & Inesi.[33] For FITC labelling, 16 μM FITC was added to 2 mg/ml of SR in a solution containing 0.3 M sucrose, 5 mM $MgCl_2$, 10 μM $CaCl_2$, 20 mM Tris-HCl (pH 8 at 20 °C). ATPase activity was measured using a coupled enzyme assay in order to monitor the labelling, which results in full inhibition at a 1:1 labelling stoichiometry;[34] labelling was complete after 10-15 minutes. Labelled SR was then diluted in an equal volume of crystallization buffer (100 mM KCl, 0.5 mM EGTA, 5 mM $MgCl_2$, 0.5 mM decavanadate, 10 μM thapsigargin) and dialyzed against this crystallization buffer for four to five days in microdialysis buttons at 4 °C. For crystallization of unlabelled Ca^{2+}-ATPase, stock solutions of SR (30 mg/ml) were simply diluted in crystallization buffer and incubated for four to five days at 4 °C.

Electron microscopy

After crystallization, samples were diluted five- to ten-fold, applied to grids coated with perforated carbon films and frozen by plunging into liquid ethane. Long,

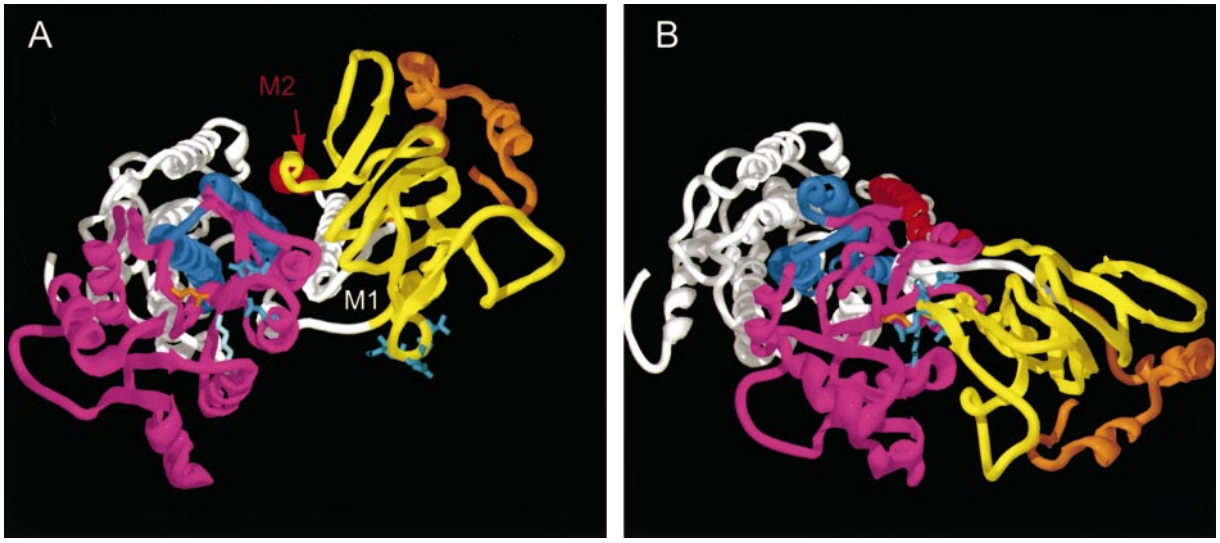

Figure 6. Rotation of the β-domain. Although this is a comparison of the X-ray structure 1EUL in (a) the E1 state with (b) our model of the E2 state, we propose that a similar rotation occurs during the E1P to E2P transition. Cyan side-chains are shown for the conserved TGES sequence in the β-domain (yellow) and for the catalytic residues D704, D707, K684 in the P-domain (magenta); D351 is orange. After rotation, these residues are brought close together, pulling M2 (red) and M1 into a different position relative to other transmembrane helices. The N-domain has been removed for clarity.

straight tubes that were suspended over holes in the carbon film were imaged in the frozen-hydrated state at 50,000× magnification and with 0.8-1.4 μm defocus. Narrow tubes (~600 Å) were screened by optical diffraction and those with sharp, symmetric layer-lines that appeared to reflect one of the helical symmetries in Table 1 were digitized at 7 μm intervals.

Image processing

Computer analysis of tubes followed procedures that have been described.[7,35,36] Briefly, after verifying helical symmetry, the length of the helical repeat was determined by cross-correlation and the tube was divided into short segments corresponding to 1/6 of a repeat. Independent alignment parameters were determined for each segment by comparison to a reference data set. After applying these parameters to segments of 1/3 repeat, layer-line data were extracted and summed to produce near and far data sets for the entire tube. The contrast transfer function was used to correct phases and weight amplitudes prior to averaging data from all tubes within a given helical symmetry group. Unit cell parameters were determined for each tube at a radius corresponding to the middle of the bilayer and tubes were discarded from the averaged data set if the length of b differed from the mean by >1.5%. Density maps were then calculated for each of the five symmetry groups without enforcing 2-fold symmetry. Each of the two molecules composing the unit cell was masked and were aligned by cross-correlation with the corresponding molecule from the reference map (−22,6). The maps were averaged in real space and then back-transformed to Fourier space for layer-line filtering based on local 2-fold residuals (see Results and Figure 1). Inverse temperature factors of 0, 50, 75, and 100 were applied to the data and 2-fold symmetry was constrained before calculating the final maps.

Quantifying resolution

Because these helical crystals have $p2$ symmetry, 2-fold phase residuals of layer-line data sets have frequently been used to document resolution[6,8] and, to monitor the efficacy of real-space averaging.[7,37] Because the maximal error for any given phase is 90°, the phase error from a set of random phases is 45°, as seen in Table 1 and Figure 1. An alternative measure of resolution relies on cross-correlation between half data sets.[10] For this calculation, real-space averaging was used to make two maps containing approximately equal numbers of repeats: i.e. (−23,6 + −22,6) and (−21,6 + −20,6 + −19,6). After masking and aligning individual molecules from these 2-fold enforced maps, Fourier shell correlation coefficients and associated phase residuals were calculated, which have maximal values of 1.0 and 90°, respectively.

Atomic modelling

Atomic coordinates for Ca^{2+}-ATPase (1EUL)[4] were divided into four domains by breaking the peptide chain at three hinge points. In particular, D737 and K329 separated the transmembrane domain from the P-domain. N359 and R604 separated the N and P-domains, and E243, K120 and L41 separated the β-domain from the transmembrane domain. The resulting four domains were fit independently into the density map by hand using the program O.[16] Besides the overall shape of the domains, the major fitting criteria involved matching α-helices to strong columns of density in the map. For the cytoplasmic domains, we used SITUS (v. 1.3) to attempt automatic fitting.[17] We specified five codebook vectors for each domain and masked the relevant portion of the density map for the fit. Although cytoplasmic domains were treated as rigid bodies, various elements of the transmembrane domain were bent or displaced to fit strong density features in the map. Finally, the loops

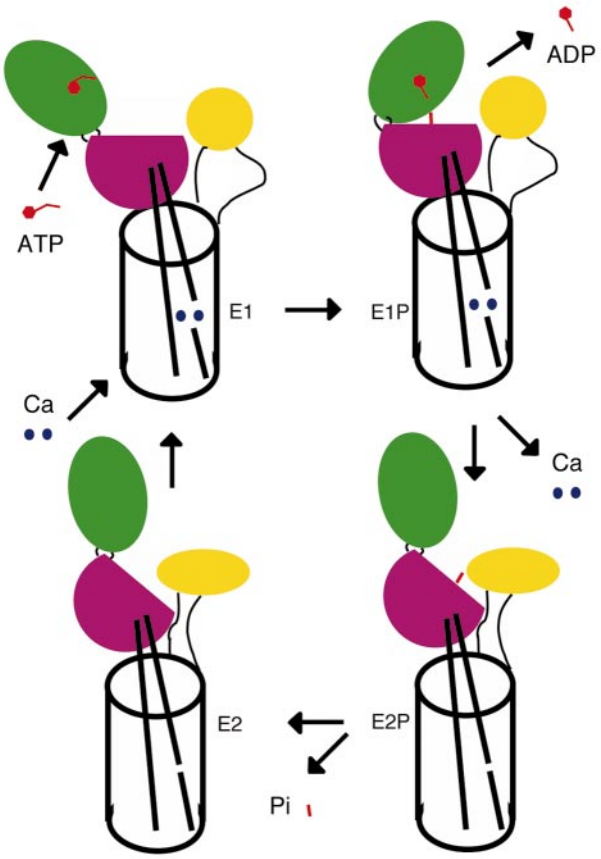

Figure 7. A cartoon summarizing the structural changes hypothesized to accompany the main steps in the reaction cycle for Ca^{2+}-ATPase. As in other Figures, the N-domain is green, the P-domain is magenta and the β-domain is yellow; the transmembrane domain is depicted as a cylinder with M4 and M5 shown as oblique lines connecting to the P-domain.

composing the three hinges were rebuilt to reconnect the domains and XPLOR was used to perform local energy minimization, thus relieving minor steric clashes that developed at domain interfaces. Despite independent fitting of the various domains, such steric clashes were very minor.

Protein Data Bank

Atomic coordinates for our E2 model have been deposited with the Protein under accession code 1KJU.

Acknowledgments

This work was supported by National Institutes of Health grant AR40997 to D.L.S. and a Canadian Institutes of Health Research fellowship to W.J.R.

References

1. Moller, J. V., Juul, B. & le Maire, M. (1996). Structural organization, ion transport, and energy transduction of ATPases. *Biochim. Biophys. Acta,* **1286**, 1-51.
2. Andersen, J. P. (1995). Dissection of the functional domains of the sarcoplasmic reticulum Ca^{2+}-ATPase by site-directed mutagenesis. *Biosci. Rep.* **15**, 243-261.
3. Inesi, G., Lu, L., Kirtley, M. E. & Takeyasu, K. (1994). Distinct structural identities of catalytic and Ca^{2+} binding domains in the sarcoplasmic reticulum ATPase. *Cell Physiol. Biochem.* **4**, 135-147.
4. Toyoshima, C., Nakasako, M., Nomura, H. & Ogawa, H. (2000). Crystal structure of the calcium pump of sarcoplasmic reticulum at 2.6 Å resolution. *Nature,* **405**, 647-655.
5. Jorgensen, P. L. & Andersen, J. P. (1988). Structural basis for E_1-E_2 conformational transitions in Na,K-pump and Ca-pump proteins. *J. Membr. Biol.* **103**, 95-120.
6. Toyoshima, C., Sasabe, H. & Stokes, D. L. (1993). Three-dimensional cryo-electron microscopy of the calcium ion pump in the sarcoplasmic reticulum membrane. *Nature,* **362**, 469-471.
7. Zhang, P., Toyoshima, C., Yonekura, K., Green, N. M. & Stokes, D. L. (1998). Structure of the calcium pump from sarcoplasmic reticulum at 8 Å resolution. *Nature,* **392**, 835-839.
8. Taylor, K. A., Dux, L. & Martonosi, A. (1986). Three-dimensional reconstruction of negatively stained crystals of the Ca^{2+}-ATPase from muscle sarcoplasmic reticulum. *J. Mol. Biol.* **187**, 417-427.
9. Bigelow, D. J. & Inesi, G. (1992). Contributions of chemical derivatization and spectroscopic studies to the characterization of the Ca^{2+} transport ATPase of sarcoplasmic reticulum. *Biochim. Biophys. Acta,* **1113**, 323-338.
10. Miyazawa, A., Fujiyoshi, Y., Stowell, M. & Unwin, N. (1999). Nicotinic acetylcholine receptor at 4.6 Å resolution: transverse tunnels in the channel wall. *J. Mol. Biol.* **288**, 765-786.
11. Pick, U. & Karlish, S. J. D. (1980). Indications for an oligomeric structure and for conformational changes in sarcoplasmic reticulum Ca^{2+}-ATPase labelled selectively with fluorescein. *Biochim. Biophys. Acta,* **626**, 255-261.
12. Csermely, P., Varga, S. & Martonosi, A. (1985). Competition between decavanadate and fluorescein isothiocyanate on the Ca^{2+}-ATPase of sarcoplasmic reticulum. *Eur. J. Biochem.* **150**, 455-460.
13. Maurer, A. & Fleischer, S. (1984). Decavanadate is responsible for vanadate-induced two-dimensional crystals in sarcoplasmic reticulum. *J. Bioenerg. Biomembr.* **16**, 491-505.
14. Stokes, D. L. & Lacapere, J.-J. (1994). Conformation of Ca^{2+}-ATPase in two crystal forms: effects of Ca^{2+}, thapsigargin, AMP-PCP, and Cr-ATP on crystallization. *J. Biol. Chem.* **269**, 11606-11613.
15. Stokes, D. L. & Green, N. M. (2000). Modeling a dehalogenase fold into the 8-Å density map for Ca^{2+}-ATPase defines a new domain structure. *Biophys. J.* **78**, 1765-1776.
16. Jones, T. A., Zou, J. Y., Cowan, S. W. & Kjeldgaard, M. (1991). Improved methods for building protein models in electron density maps and the location of errors in these models. *Acta Crystallog. sect. A,* **47**, 110-119.
17. Wriggers, W., Milligan, R. A. & McCammon, J. A. (1999). Situs: a package for docking crystal structures into low-resolution maps from electron microscopy. *J. Struct. Biol.* **125**, 185-195.

18. Wriggers, W., Agrawal, R. K., Drew, D. L., McCammon, A. & Frank, J. (2000). Domain motions of EF-G bound to the 70 S ribosome: insights from a hand-shaking between multi-resolution structures. *Biophys. J.* **79**, 1670-1678.
19. Jencks, W. P. (1989). How does a calcium pump pump calcium. *J. Biol. Chem.* **264**, 18855-18858.
20. Danko, S., Daiho, T., Yamasaki, K., Kamidochi, M., Suzuki, H. & Toyoshima, C. (2001). ADP-insensitive phosphoenzyme intermediate of sarcoplasmic reticulum Ca^{2+}-ATPase has a compact conformation resistant to proteinase K, V8 protease and trypsin. *FEBS Letters,* **489**, 277-282.
21. Sagara, Y., Wade, J. B. & Inesi, G. (1992). A conformational mechanism for formation of a dead-end complex by the sarcoplasmic reticulum ATPase with thapsigargin. *J. Biol. Chem.* **267**, 1286-1292.
22. Andersen, J. P. & Jorgensen, P. L. (1985). Conformational states of sarcoplasmic reticulum Ca^{2+}-ATPase as studied by proteolytic cleavage. *J. Membr. Biol.* **88**, 187-198.
23. Castellani, L., Hardwicke, P. M. & Vibert, P. (1985). Dimer ribbons in the three-dimensional structure of sarcoplasmic reticulum. *J. Mol. Biol.* **185**, 579-594.
24. Hardwicke, P. M. D. & Bozzola, J. J. (1989). Effect of phosphorylation on scallop sarcoplasmic reticulum. *J. Muscle Res. Cell. Motil.* **10**, 245-253.
25. Pucell, A. & Martonosi, A. (1971). Sarcoplasmic reticulum. XIV. Acetylphosphate and carbamylphosphate as energy sources for Ca^{2+} transport. *J. Biol. Chem.* **246**, 3389-3397.
26. Auer, M., Scarborough, G. A. & Kühlbrandt, W. (1998). Three-dimensional map of the plasma membrane H^+-ATPase in the open conformation. *Nature,* **392**, 840-843.
27. Ogawa, H., Stokes, D. L., Sasabe, H. & Toyoshima, C. (1998). Structure of the Ca^{2+} pump of sarcoplasmic reticulum: a view along the lipid bilayer at 9-Å resolution. *Biophys. J.* **75**, 41-52.
28. McIntosh, D. B. (1992). Glutaraldehyde cross-links Lys-492 and Arg-678 at the active site of sarcoplasmic reticulum Ca-ATPase. *J. Biol. Chem.* **267**, 22328-22335.
29. Huang, S. & Squier, T. C. (1998). Enhanced rotational dynamics of the phosphorylation domain of the Ca-ATPase upon calcium activation. *Biochemistry,* **37**, 18064-18073.
30. Patchornik, G., Goldshleger, R. & Karlish, S. J. (2000). The complex ATP-Fe^{2+} serves as a specific affinity cleavage reagent in ATP-Mg^{2+} sites of Na,K-ATPase: altered ligation of Fe^{2+} (Mg^{2+}) ions accompanies the $E_1P \rightarrow E_2P$ conformational change. *Proc. Natl Acad. Sci. USA,* **97**, 11954-11959.
31. Houdusse, A. & Sweeney, H. L. (2001). Myosin motors: missing structures and hidden springs. *Curr. Opin. Struct. Biol.* **11**, 182-194.
32. Oster, G. & Wang, H. (1999). ATP synthase: two motors, two fuels. *Structure,* **7**, R67-R72.
33. Eletr, S. & Inesi, G. (1972). Phospholipid orientation in sarcoplasmic reticulum membranes: spin-label ESR and proton NMR studies. *Biochim. Biophys. Acta,* **282**, 174-179.
34. Pick, U. & Bassilian, S. (1981). Modification of the ATP binding site of the Ca^{2+}-ATPase from sarcoplasmic reticulum by fluorescein isothiocyanate. *FEBS Letters,* **123**, 127-130.
35. Young, H., Xu, C., Zhang, P. & Stokes, D. (2001). Locating the thapsigargin binding site on Ca^{2+}-ATPase by cryoelectron microscopy. *J. Mol. Biol.* **308**, 231-240.
36. Beroukhim, R. & Unwin, N. (1997). Distortion correction of tubular crystals: improvements in the acetylcholine receptor structure. *Ultramicroscopy,* **70**, 57-81.
37. Yonekura, K., Stokes, D. L., Sasabe, H. & Toyoshima, C. (1997). The ATP-binding site of Ca^{2+}-ATPase revealed by electron image analysis. *Biophys. J.* **72**, 997-1005.

Edited by W. Baumeister

(Received 1 October 2001; received in revised form 3 December 2001; accepted 4 December 2001)